*J. Statist. Comput. Simul.*, 1995, Vol. 52, pp. 253–271
Reprints available directly from the publisher
Photocopying permitted by license only



# LONG-DURATION CORRELATION IN THE SEQUENCE OF ACTION POTENTIALS IN AN INSECT VISUAL INTERNEURON

ROBERT G. TURCOTT

*Department of Electrical Engineering, Columbia University, New York, NY 10027, USA*

PETER D. R. BARKER

*Kenneth Craik Building, Physiological Laboratory, Downing Site, Cambridge CB2 3EG, UK*

MALVIN C. TEICH

*Departments of Electrical Engineering and Applied Physics, Columbia University, New York, NY 10027, USA*

(*Received October 27, 1993; in final form January 22, 1995*)

| | |
|---|---|
| DCMD | Descending contralateral movement detector |
| DTMPP | Dead-time-modified Poisson point process |
| FFC | Fano-factor time curve |
| FSNDP | Fractal-shot-noise driven doubly stochastic Poisson point process |
| HPP | Homogeneous Poisson point process |
| ISI | Interspike interval |
| LGMD | Lobula giant movement detector |
| LSO | Lateral superior olive |
| PND | Pulse number distribution |
| PSD | Power spectral density |
| R/S | Rescaled range analysis: range/standard deviation |

Spontaneous firings of action potentials from the descending contralateral movement detector interneuron in the locust exhibit long-duration power-law correlations and therefore long-term memory. A number of statistical measures are used to establish the existence and form of the correlation, including rescaled range analysis, the pulse-number distribution, the Fano-factor time curve, and the power spectral density. This correlation may be related to the long-term sensitization observed in these cells under illumination. Long-term correlation has also been found in primary afferent auditory neurons in the cat, chinchilla, and chicken.

KEY WORDS: Long-duration power-law correlation; Descending contralateral movement detector; Spontaneous discharge; Point process; Interneuron.

## INTRODUCTION

The descending contralateral movement detector (DCMD) of the locust was so named because action potentials recorded from the ventral nerve cord (connective) are initiated by movement detected by the contralateral compound eye (Burtt & Catton, 1952, 1954). The DCMD prefers novel stimuli (Rowell and Horn, 1968) and responds strongly to objects rapidly approaching the compound eye (Rind and Simmons, 1992; Simmons and Rind, 1992). The DCMD axon makes connections in all three thoracic ganglia with interneurons and motoneurons involved in the escape jump (Burrows and Rowell, 1973; Pearson and Goodman, 1981) and with steering during flight (Simmons, 1980).

The DCMD cell body and dendrites in the protocerebrum receive visual input from a single, identified interneuron in the ipsilateral optic lobe called the lobula giant movement detector, LGMD (Rowell, 1971; Rind, 1984, 1987). It is the LGMD which gives the DCMD many of its complex visual properties (Review: Barker, 1993). Although the LGMD and DCMD have been studied extensively, the cells in the medulla which drive the LGMD have not been identified (Osorio, 1991). The cells in the medulla receive retinotopic visual input from retinal photoreceptors and large monopolar cells in the lamina.

Barker (1987, 1993) recorded and analyzed the sequences of DCMD action potentials under various scotopic conditions. In complete darkness, he showed that DCMD discharges form stationary, non-renewal processes with short-term memory that typically persists for less than 200 ms. At low light levels, the DCMD also displays longer-term memory, termed sensitization. The DCMD's sensitivity changes by up to an order of magnitude for three seconds after the presentation of a dim flash of light. The observed short-term clustering of spikes reflects correlation between spike occurrences, leading to over-dispersed distributions of interspike intervals and spike counts relative to those of a simple Poisson process. An analysis of the spike-number statistics taken from long, stable recordings showed that they are better fit by a negative-binomial than a double-Poisson (Neyman type-A) distribution, though this analysis was conducted at a single fixed counting time $T$.

In this paper we examine the counting statistics for the spontaneous DCMD discharge over a continuous range of counting times. Our results reveal the presence of long-duration correlation in the sequence of action potentials. The existence of such correlation in spike trains has been demonstrated previously for primary afferent auditory (VIII-nerve) cells in the cat (Teich and Khanna, 1985; Teich, 1989; Kumar and Johnson, 1993), chinchilla (Powers and Salvi, 1991), and chicken (Powers and Salvi, 1992), and for lateral superior olivary (LSO) neurons in the cat (Turcott *et al.*, 1994). The VIII-nerve firings are well modeled by a particular kind of stationary point process with a coincidence rate that decays as a fractional power-law function: the fractal-Gaussian-noise driven doubly stochastic Poisson point process or FGNDP (Lowen and Teich, 1991; Teich, 1992; Teich *et al.*, 1990a, 1990b; Teich and Lowen, 1994; Lowen and Teich, 1995). The spike train generated by LSO units is well modeled by an inhomogeneous Poisson point process: a sequence of randomly generated impulses whose probability of occurrence changes with time (Turcott *et al.*, 1994). At both the VIII-nerve and the LSO, correlation extends to long time scales, with an upper limit of observed correlation times imposed by the duration of the recording.



Barker (1993) has provided a detailed account of the experimental preparation. We precede our presentation of the DCMD physiological data with a thorough description of the mathematical characteristics of relevant point processes because of the unusual statistical nature of the DCMD spike trains revealed by our measurements.

## METHODS

### *1. Theoretical Background*

Since the action potentials generated by a given neuron exhibit nearly identical waveforms, the occurrence time of each action potential is generally assumed to contain the only relevant information in the sequence of neural impulses. This sequence can therefore be treated mathematically as an unmarked point process, where the occurrence of an event at time $t_i$ is represented by an impulse $\delta(t)$ at that time, so the entire realization is given by

$$s(t) = \sum_i \delta(t - t_i). \tag{1}$$

In specifying a particular realization of a point process, then, one need only specify the set of occurrence times $\{t_i\}$ of the events, as illustrated in Fig. 1A. It is useful to characterize the underlying point process from the set of occurrence times $\{t_i\}$ obtained from a single recording.

The amplitude probability distribution and correlation function of a stationary random process characterize its general behavior. For a point process the amplitude distribution is embodied in the rate of occurrence of impulses, which is readily obtained from the data, but the correlation function (or, for a point process, the coincidence rate) is generally difficult to estimate.

Because of this, two alternative reprsentations of the underlying point process are used. One perspective considers the *sequence of intervals* $\tau$, between adjacent impulses, as shown in Fig. 1B, rather than the presence or absence of an impulse at each time. In this way the point process $s(t)$ (a sequence of impulses distributed on a continuous time axis) is represented by a discrete-time random process $\{\tau_i\}$ (a sequence of positive real-valued random variables). Since $\{\tau_i\}$ is a complete representation of the point process all information can, in principle, be obtained from it. However, the mapping of the real, continuous time axis of the underlying point process to the discrete time index $i$ of the interevent time process $\{\tau_i\}$ introduces random distortion: the interval index increases by unity whether the interval is long or short. The interval subscripted by $i$ occurs, on *average*, at $t = i\ \langle\tau\rangle$, where $\langle\tau\rangle$ is the average interevent time.

As a result, some issues, particularly those concerning correlation, are more readily addressed using an alternate approach. As shown in Fig. 1C, the time axis

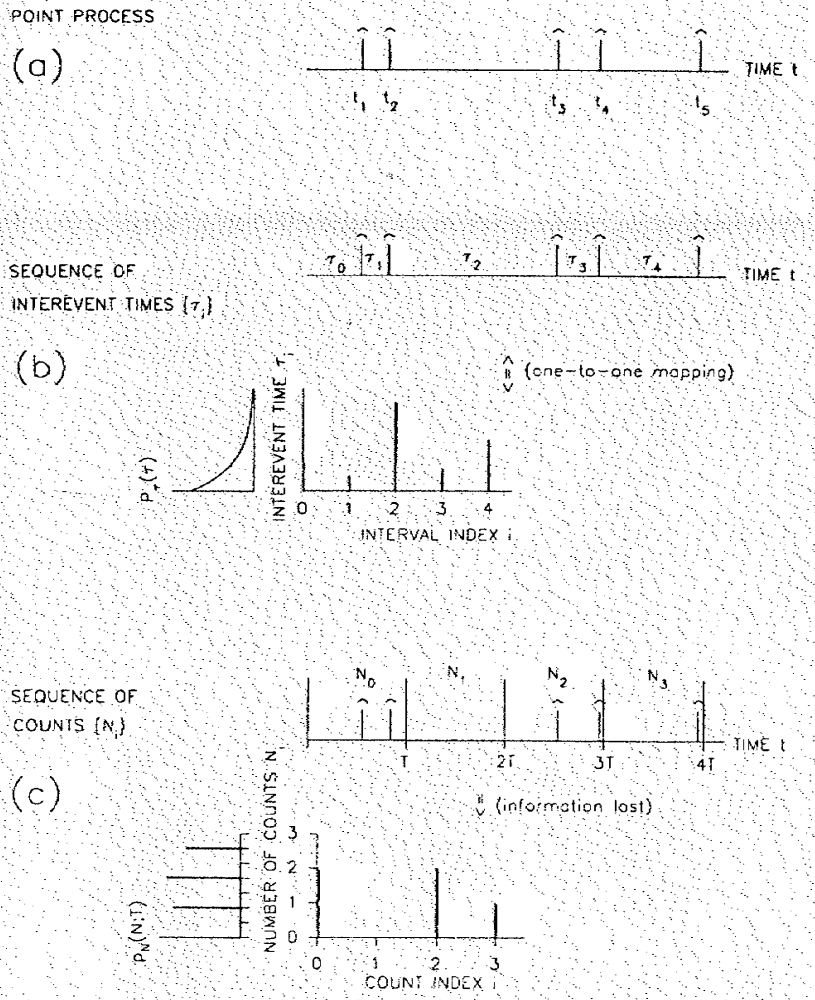


**Figure 1** Representation of the neural spike train for analysis. The sequence of action potentials is represented by a sequence of idealized impulses, forming a stochastic point process (a). The neural spike train is thus reduced to a sequence of impulse occurrence times $\{t_i\}$. For convenience of analysis two alternative representations of the point process are used. (b) A sequence of interevent times $\{\tau_i\}$ is formed from the time between impulses, resulting in a discrete-time, positive real-valued stochastic process. All information contained in the original point process is preserved in this representation, but the mapping of the point process time axis to the discrete axis of the sequence of interevent times introduces a random distortion of the abscissa. (c) The sequence of counts $\{N_i\}$, a discrete-time, non-negative integer-valued stochastic process, is formed from the point process by recording the number of events in successive counting windows of length $T$. The time axis of the point process is simply related to the discrete time axis of the sequence of counts by $t = Ti$, so correlation properties of the point process can be inferred from correlation in the sequence of counts. Information is lost in mapping the point process to the sequence of counts, but the amount lost can be made arbitrarily small by reducing the size of the counting window.





can be divided into contiguous counting periods of equal length $T$, with the number of action potentials in the $i^{th}$ window denoted $N_i$. The resulting *sequence of counts* $\{N_i\}$ forms a discrete-time random process of nonnegative integers. In general information is lost in forming this process, although for most point processes the amount lost can be made arbitrarily small by sufficiently reducing the size of the counting window $T$. One advantage of this representation lies in the link provided by the counting time $T$ between the discrete time axis of the process of counts $\{N_i\}$ and the absolute, real time axis of the underlying point process. The count index increases by unity for every $T$ seconds in the point process. With the process of counts $\{N_i\}$, $N_i$ and $N_{i+k}$ refer to the number of counts in windows separated by precisely $T(k)$ seconds, so that correlation in the process $\{N_i\}$ is readily associated with correlation in the underlying point process $s(t)$.

As a first example, we consider the homogeneous Poisson point process (HPP) which is ubiquitous, playing the role in point process theory that the Gaussian random process plays in the study of continuous-time stochastic processes (Saleh and Teich, 1982). The HPP is memoryless: the occurrence of an event at time $t_0$ is independent of the presence or absence of events at any other time $t \neq t_0$. Because of this property both $\{\tau_i\}$ and $\{N_i\}$ form sequences of independent, identically distributed (iid) random variables. These processes are completely characterized by their amplitude probability density and mass functions. In the context of neural spike-train analysis, these are typically called the interspike-interval (ISI) histogram and the count-number or pulse-number distribution (PND).

For the process $\{\tau_i\}$ generated from an HPP the amplitude probability density function is the simple exponential

$$p_\tau(\tau) = \lambda e^{-\lambda\tau}, \tag{2}$$

where $\lambda$ is the average number of events per unit time. The probability mass function $p_N(n; T)$ of the amplitude of the count process $\{N_i\}$ is the Poisson distribution

$$P_N(n; T) = \frac{(\lambda T)^n e^{-\lambda T}}{n!}, \tag{3}$$

which has the property that for all counting times $T$ the variance $\sigma^2_{N,T}$ is equal to the mean $\mu_{N,T}$ of the number of counts: $\sigma^2_{N,T} = \mu_{N,T} = \lambda T$.

A point process whose interevent times form a sequence of iid random variables is said to be renewal, a definition motivated by the study of processes generated by the replacement of failed parts (e.g., light bulbs). Each replacement forms a renewal of the point process. The HPP is the only point process with a finite rate for which the sequence of counts consists of independent random variables for all counting times. Since the HPP is the renewal process whose interevent density function $p_\tau(\tau)$ is exponential, any departure of $p_\tau(\tau)$ from exponential in a renewal process implies the existence of memory in the underlying point process. In the sequence of counts, this memory results in dependence among the $\{N_i\}$.

Random shuffling of the sequence of interevent times $\{\tau_i\}$ preserves the proba-

bility density function $p_\tau(\tau)$ characterizing the amplitude of the interval process, but destroys the correlation among intervals. Shuffling therefore provides a convenient method for generating a realization of a renewal process whose $p_\tau(\tau)$ is identical to that of the data. In general, a point process can have memory even if its sequence of interevent times is renewal. Comparison of the original data and the shuffled intervals makes clear which properties of the data arise from correlation among intervals and which properties can be accounted for by the form of the interval probability density function.

### 2. *Statistical Measures*

Probability theory allows the characterization of the random variables of a given stochastic model in terms of probability distributions and correlation functions, which in turn, allows the prediction of the outcome of an experiment using that model. In the analysis of empirical data the problem is approached from the opposite direction: given a collection of empirical data, the probabilistic functions are estimated, with the ultimate aim of modeling the physiological process with a mathematical stochastic system.

We utilize two statistical measures that partially characterize the random process in terms of a sequence of interspike *intervals* $\{\tau_i\}$: the interspike-interval (ISI) histogram and rescaled range analysis (R/S).

The ISI histogram shows the relative frequency of occurrence of interspike intervals as a function of interval size; it is an estimate of the probability density function $p_\tau(\tau)$ of the amplitude of $\{\tau_i\}$. The ISI histogram readily provides information about the underlying process over short time scales, but all information regarding the order of interval occurrence is lost. If no correlation exists among the interspike intervals then the process formed by the sequence of interevent times $\{\tau_i\}$ is renewal, and the point process is completely characterized by its ISI histogram. Conversely, if the process is nonrenewal (i.e., if dependence exists among its interevent intervals) then the ISI histogram does not completely characterize the point process. In that case, measures that reveal the nature of the correlation provide complementary information to the ISI histogram.

The survivor function and the hazard function are transformations of $p_\tau(\tau)$ commonly used in neuronal spike-train analysis (Perkel *et al.*, 1967). The survivor function $\mathcal{S}_\tau(\tau)$ is the complement of the ISI cumulative probability distribution.

$$\mathcal{S}_\tau(\tau) \equiv 1 - F_\tau(\tau) = 1 - \int_0^\tau p_\tau(x)\,dx. \tag{4}$$

It provides the probability that the neuron will not have fired within $\tau$ seconds of the preceding action potential. The hazard function, defined as

$$\phi_\tau(\tau) \equiv p_\tau(\tau)/\mathcal{S}_\tau(\tau), \tag{5}$$

gives the probability that the neuron will fire $\tau$ seconds after an action potential,



given that no action potential has occurred during this $\tau$ seconds. For an HPP with rate $\lambda$ the survivor function is the exponential $\mathcal{S}_\tau(\tau) = e^{-\lambda\tau}$, and the hazard function is a constant given by the rate, i.e., $\phi_\tau(\tau) = \lambda$.

Rescaled range analysis provides information about correlation among interspike intervals. It is particularly well suited to processes that exhibit long-term correlation or that have large or infinite variance (Hurst, 1951; Feller, 1951; Mandelbrot, 1983; Teich *et al.*, 1990b). For a block of $k$ intervals, the difference between each interval and the average interval size is obtained and successively added to a cumulative sum. The normalized range $R(k)$ is the difference between the maximum and minimum values that the cumulative sum attains, divided by the standard deviation of the interval size. Information about the nature and degree of correlation in the process is obtained by fitting $R(k)$ with the function $k^h$. If $h > 0.5$ then positive correlation exists among the intervals, while $h < 0.5$ indicates the presence of negative correlation, in which an interval that is larger than the mean tends, on the average, to be preceded by or followed by one smaller than the mean.

For the random process formed by the sequence of *counts* from DCMD interneurons, we apply three measures. The pulse-number distribution (PND) provides an estimate of the probability mass function of the amplitude of the sequence of counts $\{N_i\}$. It reveals the character of the point process on time scales that are of the order of the counting time $T$. Since the counting time is externally specified, the behavior of the point process for arbitrary time scales can be examined. The Fano factor, defined as the count variance divided by the count mean, is a useful index of dispersion since its value for the HPP is unity for all $T$ (Cox and Lewis, 1966). A Fano factor greater than unity indicates that the underlying point process is more clustered than the HPP at the given time scale, whereas a Fano factor less than unity indicates that the underlying point process is more regular than the HPP. Aside from the Fano factor, the characteristics of the PND provide other information about the underlying point process. A higher probability of an even number of counts than an odd number of counts in a interval of length $T$, for example, implies that events tend to occur in pairs separated by less than $T$ seconds (Teich and Turcott, 1988). In this way the PND at a particular counting time, and the Fano factor, provide information about the correlation of the point process at that time scale (Teich and Khanna, 1985).

The Fano-factor time curve (FFC), which shows the functional dependence of the Fano factor on the counting time $T$, provides additional information about the nature of the correlation. In particular, an FFC with a power-law dependence on $T$ implies that the underlying point process has a power-law correlation function (normalized coincidence rate for a point process) and power spectral density (Teich, 1989, 1992).

Since the FFC is related to the normalized coincidence rate through an integral transformation (Teich, 1992), its value at a particular counting time $T$ is influenced by correlation across all time scales. Because of this, even weak correlation can produce dramatic departures of the Fano factor from unity (Teich, 1989, 1992). This property imparts the FFC with particular sensitivity to correlation in a point process.

Finally, Fourier transform methods provide an alternative approach to quantifying

the correlation of a stochastic process. We use a periodogram estimate $S(f)$ of the power spectral density (PSD) of the sequence of counts $\{N_i\}$, given by

$$S(f) \equiv \frac{1}{M} |X(f)|^2, \tag{6}$$

where $M$ is the number of samples and $X(f)$ is the discrete Fourier transform of the stochastic process (Papoulis, 1984; Press *et al.*, 1988). Information can be inferred about time correlation from the PSD since it is simply a linear transformation of the autocorrelation function of the process.

## RESULTS

The recordings of DCMD spontaneous action-potential firings analyzed here have been previously shown to form stationary processes (Barker, 1993; Barker, unpublished results). The duration, number of intervals, and average firing rate for each of the recordings discussed in this paper are shown in Table 1. Two additional data sets that were analyzed yielded results similar to those reported here.

The ISI histogram for each data set is presented in Fig. 2 (solid curves). The ISI histograms have an exponential form for long interevent times (they are well represented by straight lines on the semilogarithmic plots of Fig. 2A), and a power-law form for short interevent times (straight lines on the doubly logarithmic plots of Fig. 2B), with the transition between the two regions occurring at approximately $\tau = 1$ sec.

The decreasing relative frequency for very short interevent times (less than approximately 20 ms), shown in Fig. 2B, indicates the presence of refractoriness. The ISI histogram extends out to long interevent times because of the low spontaneous firing rates.

The function

$$p_\tau(\tau) = \begin{cases} c_1 \tau^{-\gamma} & \tau \le \tau_0 \\ c_2 e^{-\lambda \tau} & \tau > \tau_0, \end{cases} \tag{7}$$

**Table 1** Characteristics of four long-duration recordings from spontaneously firing DCMD neurons. The parameters $\alpha$ and $\beta$ are the exponents obtained from fitting the functions $F(T) = AT^{\alpha}$ and $S(f) = Bf^{-\beta}$ to the FFC and PSD, respectively. As expected from theory (Teich, 1992; Lowen and Teich, 1995), $\beta \approx \alpha$.

| *Cell Identification* | *Duration of recording (sec)* | *Number of Intervals* | *Average Firing Rate ($sec^{-1}$)* | *FFC exponent $\alpha$* | *PSD exponent $\beta$* |
|---|---|---|---|---|---|
| ADA011 | 5217.5 | 3524 | 0.680 | 0.180 | 0.203 |
| ADA034 | 2356.1 | 3331 | 1.41 | | |
| ADA062 | 7886.1 | 4070 | 0.516 | 0.149 | 0.150 |
| ADA072 | 3806.3 | 4555 | 1.20 | | |



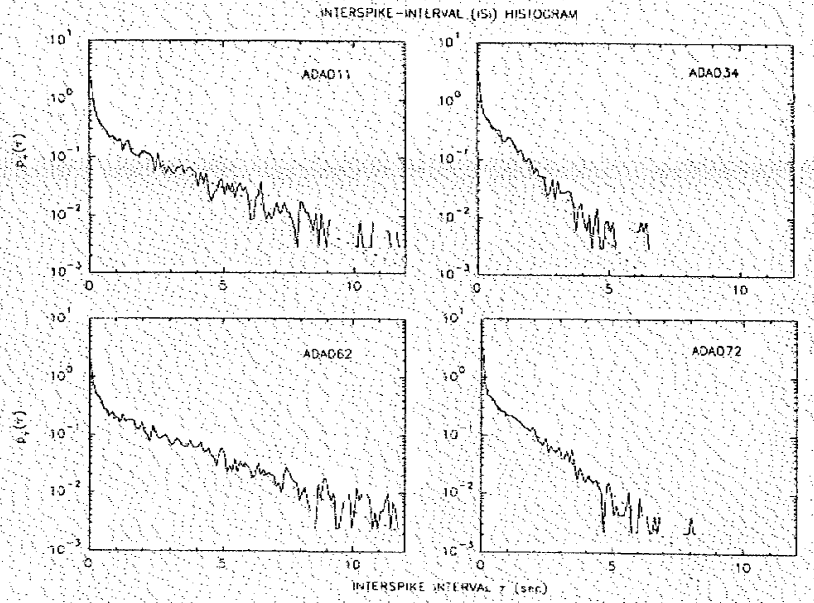


**Figure 2** Interspike-interval (ISI) histograms for four spontaneously firing DCMD cells. The data are shown on a semilogarithmic plot in (A) and on a doubly logarithmic plot with an expanded view of short time intervals in (B) (see next page). The ISI histograms (solid curves) are well described by power-law functions for short time scales ($\tau < 1$ sec) [straight-line behavior in (B)] and by exponential functions for long time scales [straight-line behavior in (A)]. This behavior, represented by Eq. (7), is plotted as the dotted curves in Fig. 2(A) and (B). The algorithm used to find the best fit of the function to the data did not impose continuity at $\tau_0 = 1$ sec.

with $\tau_0 = 1$ sec, was fit to the ISI histograms using the Marquardt-Levenberg algorithm. The best fitting parameters are presented in Table 2, and the corresponding functions are plotted in Fig. 2 as dotted curves. This function describes the data very well in both regions. The greatest discrepancy occurs in cell ADA072 in the power-law region. For $0.01 < \tau < 1$ sec, the ISI histogram for this cell diverges slightly from a straight line on the doubly logarithmic plot so a simple power-law function serves only as an approximation.

The survivor functions and hazard functions, which are often-used measures in neurophysiological spike-train analysis, are presented in Figs. 3A and 3B respectively. The abscissa values of the survivor function are obtained directly from the data. This minimizes noise in the plot, since it is not based on a conventional histogram with externally specified bin widths. Because the fit of Eq. (7) to the data was based solely on the functional form of the data, the fitting algorithm did not incorporate a normalization condition. Equation (7), therefore, does not nec-

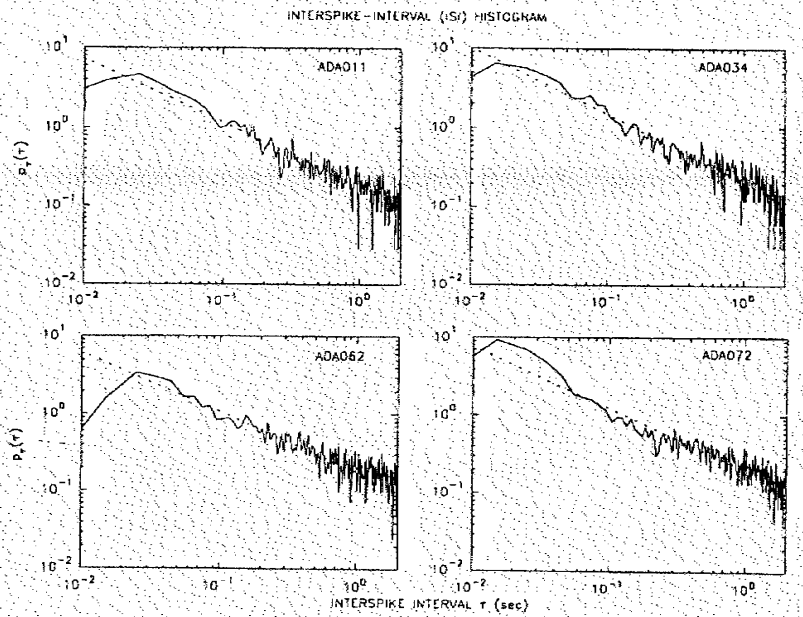


**Figure 2** (continued)

essarily transform properly to the survivor and hazard functions, which implicitly require normalization. With this caveat in mind, the dotted lines in Fig. 3B are obtained from the exponential tails of Eq. (7). For long interspike intervals, the data appear to be reasonably well modeled by an exponential ISI probability density function. The excess probability of short intervals relative to an exponential is clearly apparent in the hazard functions of Fig. 3B.

The rescaled range analysis of each data set is presented in Fig. 4. The circles correspond to the result for uncorrelated intervals $R(k) \sim k^{1/2}$ for comparison with the data. Correlation among interspike intervals is present in all the data sets (solid

**Table 2** Parameters obtained by fitting Eq. (7), with $\tau_0 = 1$ sec, to the ISI histograms of the DCMD data.

| *Cell Identification* | $c_1$ | $\gamma$ | $c_2$ | $\lambda$ |
|---|---|---|---|---|
| ADA011 | 0.188 | 0.795 | 0.283 | 0.451 |
| ADA034 | 0.217 | 0.835 | 0.730 | 1.040 |
| ADA062 | 0.179 | 0.777 | 0.305 | 0.416 |
| ADA072 | 0.203 | 0.791 | 0.539 | 0.801 |



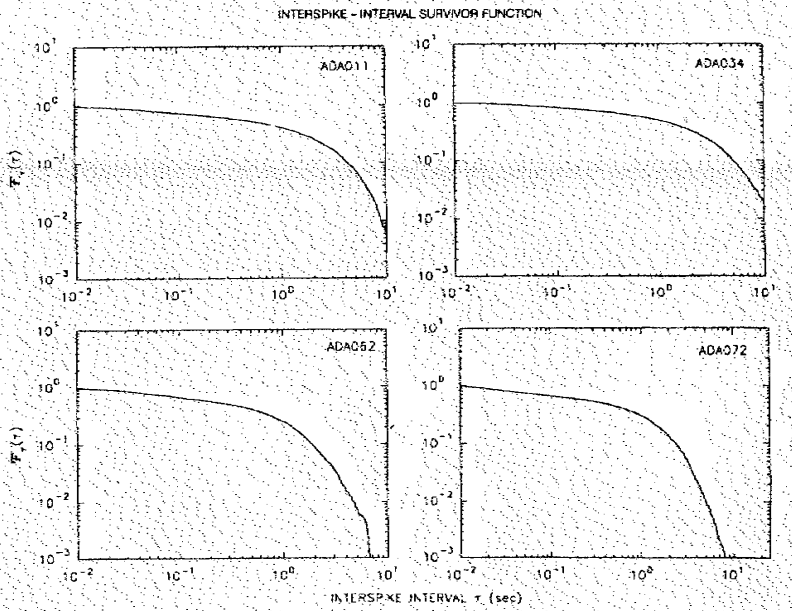


**Figure 3** Interspike-interval (ISI) survivor functions (A) and hazard functions (B) (see next page). The theoretical hazard function obtained from an exponentially distributed ISI is a constant. The dotted line in (B) is the hazard function expected for the exponential tail in Eq. (7). The excess of short ISIs relative to the exponential is apparent.

curves) since $R(k)$ grows more rapidly than $k^{1/2}$. The correlation appears particularly strong when the block size approaches several hundred intervals. The correlation present for large $k$ is destroyed by randomly shuffling the intervals. $R(k)$ curves for the shuffled intervals are shown as dashed curves in Fig. 4, which have $R(k)$ approximately proportional to $k^{1/2}$ as expected. These findings are consistent with the interval serial correlation coefficients reported by Barker (1993). For purposes of comparison, a dead-time-modified Poisson point process (DTMPP), an HPP with absolute refractoriness imposed, was simulated for each data set and rescaled range analysis was applied to each. The mean of the DTMPP, and the duration of the simulation, were taken to be the same as that of the data. The dead time was taken to be 10 msec. The behavior of $R(k)$ for the simulated DTMPP (dotted curves) and the shuffled intervals is qualitatively similar. This is as expected since all renewal processes, regardless of the form of their ISI histograms, should exhibit an $R(k)$ proportional to $k^{1/2}$, a consequence of the fact that R/S reveals correlation among intervals, not correlation in time.

We now move to results for the counting process. The PNDs obtained from the

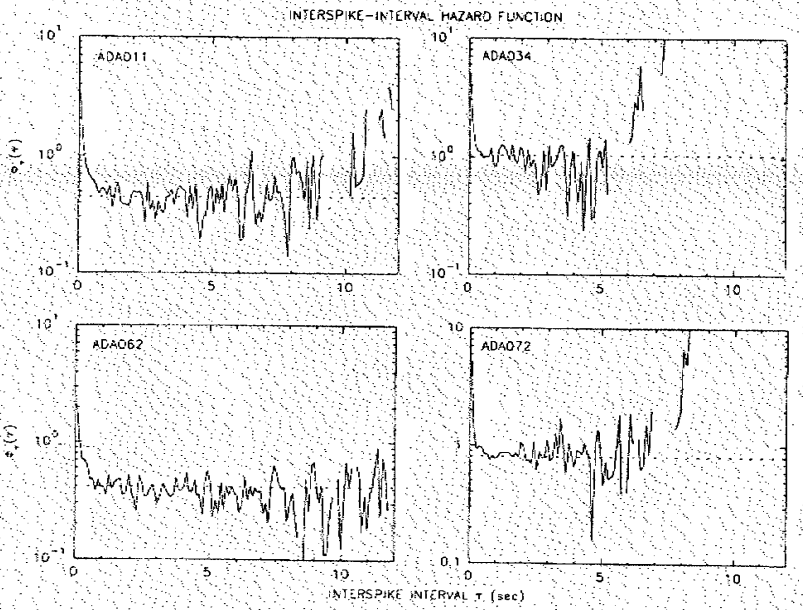


**Figure 3** (continued)

data, using a counting time of $T = 2.5$ sec, are presented in Fig. 5 (solid curves). PNDs obtained from simulated DTMPPs, with the same mean and an absolute refractory period of 10 msec, are plotted as dotted curves. In each case the PND of the data has a greater dispersion than that of the DTMPP. This is quantified in the Fano factor, $F(T)$, defined as the variance divided by the mean. $F(T)$ greater (less) than unity indicates the PND calculated at that counting time $T$ has more (less) dispersion than the PND of an HPP.

The Fano-factor time curves for the data are shown as the solid curves in Fig. 6. The increase of the Fano factor with counting time indicates that the underlying sequence has greater count variability, and is hence more clustered, than a homogeneous Poisson process. The FFCs show various regions of power-law behavior (straight-line appearance on a doubly logarithmic plot). For the spontaneous discharges from cells ADA011 and ADA062 the exponent of the data is approximately constant over more than two decades of the counting time. The power-law function $F(T) = AT^{\alpha}$ was fit to these data using the Marquardt-Levenberg algorithm, and is shown in the figure as open circles. The best-fitting FFC exponents (parameter $\alpha$) are presented in Table 1. Spontaneous discharges from cells ADA034 and ADA072, which have the highest firing rates, exhibit more complex behavior with different regions exhibiting different power-law exponents.

The FFCs obtained from the equivalent renewal process (obtained by shuffling



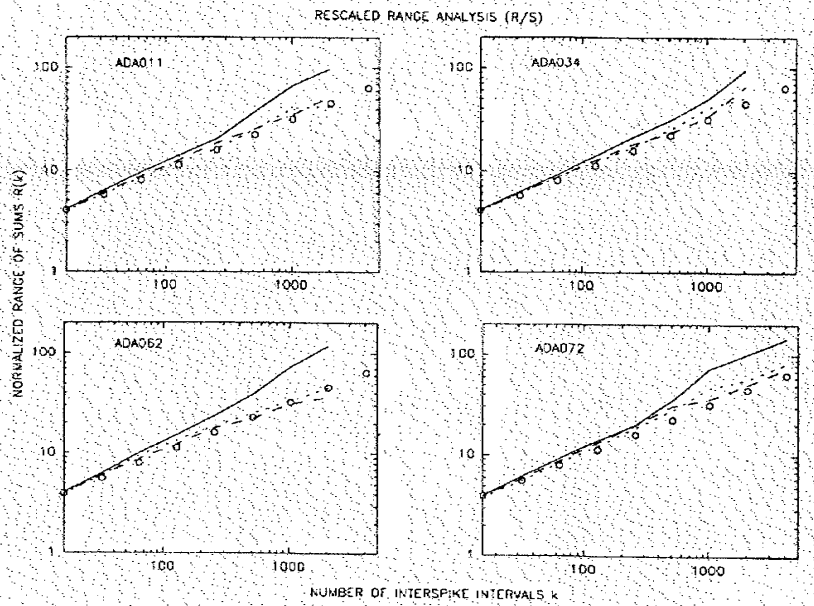


**Figure 4** Rescaled range analysis (R/S) applied to the neurophysiological data (solid curves), to the process formed by shuffling the intervals (dashed curves), and to a simulated DTMPP (dotted curves). The data show strong positive correlation for large blocks of intervals $k$. The shuffled process and the DTMPP appear uncorrelated, which is expected since both are renewal processes with interspike intervals drawn independently from their respective ISI histograms. The circles correspond to the theoretical result for uncorrelated intervals $R(k) \sim k^{1/2}$ for comparison with the data.

the intervals) are shown as the dashed curves in Fig. 6. The increase above unity in the FFC of the process of shuffled intervals arises entirely from the departure of the ISI histogram from exponential form. Note that the FCC for the shuffled intervals is approximately constant for counting times greater than a typical interspike interval. This indicates that the counts are uncorrelated on these time scales (Teich *et al.*, 1990b; Turcott *et al.*, 1994), which is to be expected since the count correlation in a renewal process cannot extend beyond the largest interspike interval.

Also shown in Fig. 6 are the FFCs obtained from the simulated DTMPP (dotted curves). The effect of dead time on the FFC is negligible since the refractory period is small relative to the average interevent time. For the DTMPP under these conditions, $F(T)$ is approximately unity for all counting times. Point processes with more prevalent dead time would dip below unity at the time scale of the dead time (Teich, 1992).

Finally, in Fig. 7 we present the periodograms generated from the sequence of

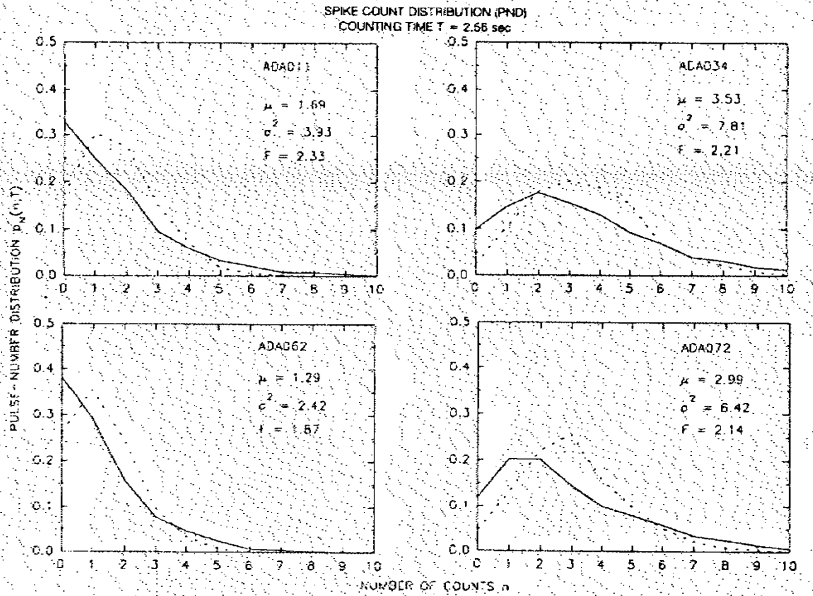


**Figure 5** Pulse-number distributions (PNDs) for the data (solid curves) and simulated DTMPP (dotted curves), with $T = 2.5$ sec. The mean, variance, and Fano factor (variance-to-mean ratio) are given in each panel. The data exhibit wider distributions than the DTMPP, and indeed the value of the Fano factor is greater than unity, indicating that the variance of the data is greater than that of the DTMPP (the means of both are equal). The greater dispersion implies more clustering in the underlying point process than is present in an HPP or a DTMPP. The clustering is a manifestation of correlation. Barker (1993) presents an analysis of the null hypothesis that these distributions arise from a Poisson point process.

counts $\{N_i\}$ using a counting time of $T = 0.02$ sec. The periodograms obtained from the data are shown as solid curves, those from the shuffled intervals as dashed, and those from the simulated DTMPPs as dotted. The divergence of $S(f)$ from a horizonal line (white noise) indicates the presence of correlation among the sequence of counts. In particular, the form of $S(f)$ is power law over a range of frequencies, consistent with the presence of power-law correlation indicated by the FFC. Power-law functions $S(f) = Bf^{-\beta}$ were fit to the PSDs of cells ADA011 and ADA062. These are shown as circles in the figure, and the best-fitting power-law exponents (parameter $\beta$) are presented in Table 1.

## DISCUSSION

The statistical behavior of the four DCMD units we present is qualitatively very similar. The form of the ISI histogram (Fig. 2) is remarkably consistent among the



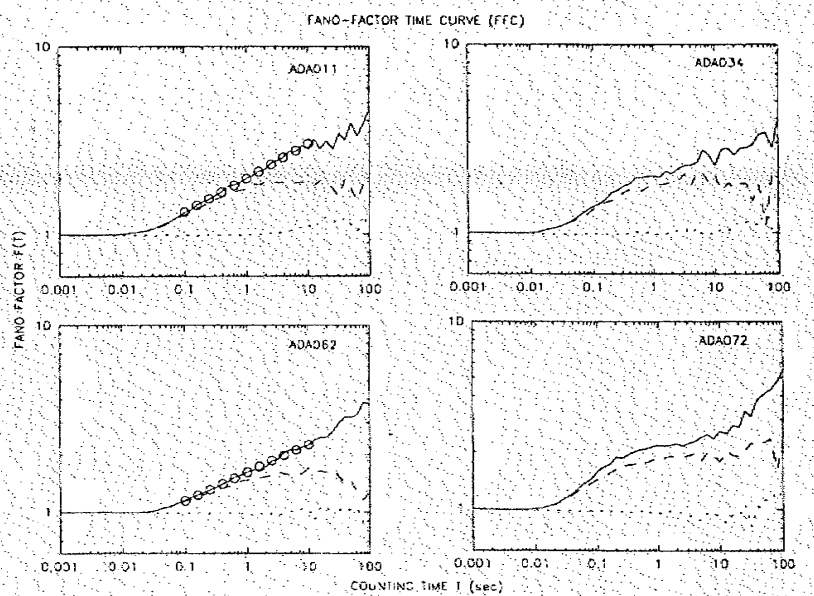


**Figure 6** Fano-factor time curves (FFCs) for the data (solid curves), shuffled intervals (dashed curves), and simulated DTMPPs (dotted curves). A departure of the FCC from unity indicates the presence of correlation in the sequence of counts. The difference between the FFC of the data and that of the shuffled process is entirely due to correlation among the intervals, which is destroyed by shuffling. The residual correlation apparent in the FFC of the shuffled process arises from the departure of the ISI histogram from an exponential form, in this case manifested by the excess of short interevent times relative to the HPP, as revealed in Fig. 2. The FFC appears to follow a fractional power law for certain ranges of counting time $T$, implying than the underlying point process has power-law correlation on the corresponding time scales. Data from cells ADA011 and ADA062 were fit with the function $F(T) = AT^{\alpha}$, yielding $\alpha = 0.180$ and $\alpha = 0.149$, respectively. These functions are shown as open circles in the figure. The FFCs of cells ADA034 and ADA072 show more complex power-law behavior.

data sets, each having an exponential form for long interevent times with an excess of short intervals relative to the ISI for the HPP. The existence of long-term correlation in all the data sets is clear from the R/S (Fig. 4), PND (Fig. 5), FFC (Fig. 6), and PSD (Fig. 7) analyses.

Subtle differences do exist among the recordings, however. The ISI histogram for cell ADA072 is not quite as well fit by a power-law function on short times scales as are the other cells (Fig. 2). The FFCs for cells ADA011 and ADA062 are arguably power-law for $T$ greater than approximately 30 msec (Fig. 6). For $T > 20$ msec, the data from ADA034 and ADA072 appear to have various power-law exponents in their FFCs. The power-law exponent of ADA034 is greater for 20 msec $< T <$ 500 ms than for $T >$ 500 ms. The data for ADA072 exhibit three regions: 20 msec $< T <$ 300 msec; 300 msec $< T <$ 10 sec; $T >$ 10 sec, with the

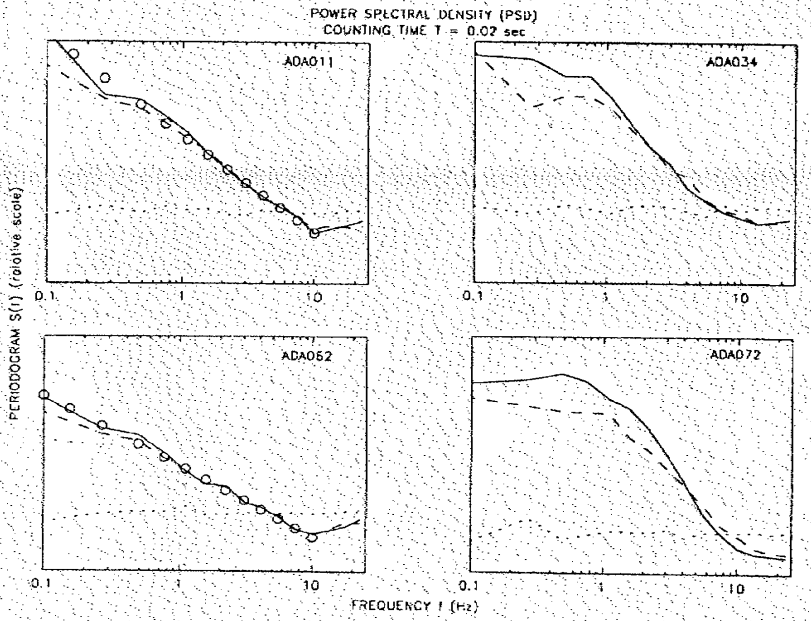


**Figure 7** Periodogram estimates of the power spectral density (PSD), shown for the data (solid curves), shuffled intervals (dashed curves), and simulated DTMPPs (dotted curves). Each data set was divided into successive segments of 20.48-sec blocks of data. For each segment, 1024-point periodograms were formed from the sequence of counts using a counting time $T = 0.02$ sec. The periodograms of each segment were averaged. Further variance reduction was accomplished by averaging adjacent frequency bins of the PSD estimate. The PSD of the data shows regions of power-law form, consistent with the results obtained from the FFC. The data from cells ADA011 and ADA062 were fit with the function $S(f) = Bf^{-\beta}$, yielding $\beta = 0.203$ and $\beta = 0.150$, respectively, consistent with the theoretical prediction that the exponents of the PSD be (approximately) equal in magnitude, but opposite in sign, from those of the FFC. The functions corresponding to the best-fitting parameters are shown as circles in the figure. The PSDs of ADA034 and ADA072 reflect more complex behavior as observed in the corresponding FFCs.

power-law exponent moderate in the first region, small in the middle region, and large for $T > 10$ sec. This difference in the form of the FFC among the data sets suggests that there may be two classes of DCMD cells. In addition to the results presented here, data from two other cells were analyzed. One (ADA058) appears to have a single power-law region, like ADA011 and ADA062. The other (ADA067) appears to have various regions, similar to ADA034 and ADA072.

Regions of power-law behavior in the FFC correspond to time scales of the underlying point process that have power-law correlation. These results therefore indicate that the spontaneous firings of DCMD cells exhibit power-law correlation.



Correlation in the spike train extends to the largest time scales that could be examined with satisfactory statistical accuracy (approximately 100 sec). Long-duration power-law correlation imparts fractal-like behavior to the firing rate (Teich *et al.*, 1990a; Teich, 1992), which exhibits large, scale-invariant fluctuations.

Because the FFCs for cells ADA011 and ADA062 are well described by simple power-law functions at long time scales (Fig. 6), the corresponding PSDs reflect the simple form of these FFCs, and therefore exhibit large regions of power-law decay (Fig. 7). The best-fitting power-law exponent ($\beta$) is approximately equal in magnitude to that of the FFC ($\alpha$), consistent with theoretical predictions (Teich, 1989; Teich, 1992; Lowen and Teich, 1995) (Table 1). The complexity in the FFCs of ADA034 and ADA072 is reflected in the complex form of the corresponding PSDs. In all cases, however, regions of power-law behavior in one of the measures can be associated with regions of power-law behavior in the other.

For the spike trains examined here, the departure of the ISI histogram from an exponential function for short interevent times ($\tau < 1$ sec) (Fig. 2B) accounts for the correlation evident in the FFC as well as PSD measures obtained from the shuffled data sets (dashed curves in Figs. 6 and 7). The difference between the original-data and the shuffled-data curves arises entirely from the order of occurrence of the intervals.

The correlation in spontaneous DCMD firings bears some similarity to that observed in a number of other neurophysiological preparations. In the retinal ganglion cell of the cat, Levine (1980) showed that the standard deviation of the random variable that serves as the rate has a power-law dependence on counting time. Since the rate is simply the number of counts divided by the counting time, these results translate into a power-law FFC for large counting times. The correlation in the retinal ganglion cell observed by Levine is relatively weak, however, inasmuch as the FFC (which lies below unity for short counting times as a result of refractoriness) never rises above unity for any of the counting times reported (which were as long as 20 sec). The FFC of DCMD cells is similar to that measured in primary auditory neurons of the cat (Teich, 1989; Teich *et al.*, 1990a,b; Teich, 1992; Kumar and Johnson, 1993), but the FFCs of the shuffled data and the ISI histograms differ in the two cases. The auditory data is well modeled by a fractal-Gaussian-noise driven doubly stochastic Poisson point process (FGNDP; Lowen and Teich, 1991; Teich *et al.*, 1990b; Teich, 1992; Teich and Lowen, 1994). The FGNDP can be derived from a cascade model, in which each occurrence of an event in a primary point process generates a number of secondary events (Lowen and Teich, 1991).

Barker (1993) has used a nonfractal version of the cascade model to describe firings in DCMD cells, in which an additional element of randomness is incorporated into the generation of the secondary events. This model was first set forth by Saleh and Teich (1982, 1985). In terms of Barker's model, the values of $\gamma$ and $\lambda$ shown in Table 2 are associated with the degree of temporal clustering of the secondary process and the rate of the primary process, respectively. However, the nonfractal SNDP model cannot account for power-law growth of the FFC.

Barker (1993) has demonstrated the presence of sensitization in the DCMD: a brief stimulus elicits an enhanced response when it follows another stimulus within

three seconds. This sensitization may well result from the same mechanism that produces the long-duration correlation exhibited in the FFC of spontaneous firings.

Whatever the mechanism, however, it is clear that power-law correlation, and hence long-term memory, is present in the spike trains associated with these cells.

## *Acknowledgments*

This work was supported by the Office of Naval Research under Grant N00014-92-J-1251 and by the Joint Services Electronics Program through the Columbia Radiation Laboratory.

## *References*

Barker, P. D. R. (1987). Statistics of spike discharges from a visual unit in the locust, PhD Dissertation. Cambridge University (U.K.).

Barker P. D. R. (1993). Sensitization and multiplicative noise in the descending contralateral movement detector (DCMD) of the locust. *Vis. Neurosci.*, **10,** 791–809.

Burrows, M., Rowell, C. H. F. (1973). Connections between descending visual interneurons and metathoracic motoneurons in the locust. *J. Comp. Physiol.*, **85,** 221–234.

Burtt, E. T., Catton, W. T. (1952). Nerve impulses originating from the compound eye of the locust. *Nature*, **170,** 285.

Burtt, E. T., Catton, W. T. (1954). Visual perception of movement in the locust. *J. Physiol.*, **125,** 566–580.

Cox, D. R., Lewis, P. A. W. (1966). The statistical analysis of series of events. Chapman and Hall, London.

Feller W. (1951). The asymptotic distribution of the range of sums of independent random variables. *Ann. Math. Stat.*, **22,** 427–432.

Hurst, H. E. (1951). Long-term storage capacity of reservoirs. *Trans. Amer. Soc. Civil Eng.*, **116,** 770–808.

Kumar, A. R., Johnson, D. H. (1993). Analyzing and modeling fractal intensity point processes. *J. Acoust. Soc. Am.*, **93,** 3365–3373.

Levine, M. W. (1980). Firing rates of a retinal neuron are not predictable from interspike interval statistics. *Biophys. J.*, **30,** 9–25.

Lowen, S. B., Teich, M. C. (1991). Doubly stochastic Poisson point process driven by fractal shot noise. *Phys. Rev. A.*, **43,** 4192–4215.

Lowen, S. B., Teich, M. C. (1995). Estimation and simulation of fractal stochastic point processes. *Fractals*, **3,** Issue No. 1 (in press).

Mandelbrot, B. B. (1983). The fractal geometry of nature. Freeman, New York.

Osorio, D. (1991). Patterns of function and evolution in the arthropod optic lobe. In: Cronly-Dillon, J. R., Gregory, R. (eds). Vision and visual dysfunction. Volume II: Evolution of the eye and visual system. Macmillan, London.

Papoulis, A. (1965, 1984). Probability, random variables, and stochastic processes. McGraw-Hill, New York.

Pearson, K. G., Goodman, C. S. (1981). Presynaptic inhibition of transmission from identified interneurones in the locust central nervous system. *J. Neurophysiol.*, **45,** 501–515.

Perkel, D. H., Gerstein, G. L., Moore, G. P. (1967). Neuronal spike trains and stochastic point processes I. The single spike train. *Biophys. J.*, **7,** 391–418.

Powers, N. L., Salvi, R. J., Saunders, S. S. (1991). Discharge rate fluctuations in the auditory nerve of the chinchilla, Abstracts of the XIV Midwinter Research Meeting, Assoc. for Res. In Otolaryngology, Des Moines, IA, Abstract No. 411, p. 129.

Powers, N. L., Salvi, R. J. (1992). Comparison of discharge rate fluctuations in the auditory nerve of chickens and chinchillas, Abstracts of the XV Midwinter Research Meeting, Assoc. for Res. in Otolaryngology, Des Moines, IA, Abstract No. 292, p. 101.

Press, W. H., Flannery, B. P., Teukolsky, S. A., and Vetterling, W. T. (1988). Numerical recipes in C. Cambridge University Press, New York.



Rind, F. C. (1984). A chemical synapse between two motion detecting neurones in the locust brain. *J. Exper. Biol.*, **110,** 143–167.

Rind, F. C. (1987). Non-directional, movement sensitive neurones of the locust optic lobe. *J. Comp. Physiol. A*, **161,** 477–494.

Rind, F. C., Simmons, P. J. (1992). The orthopteran DCMD neuron: a re-evaluation of responses to moving objects. I. Selective responses to approaching objects. *J. Neurophysiol.*, **68,** 1654–1666.

Rowell, C. H. F. (1971). The orthopteran descending movement-detector (DCMD) neurons: a characterisation and review. *J. Comp. Physiol.*, **73,** 167–194.

Rowell, C. H. F., Horn, G. (1968). Dishabituation and arousal in the response of single nerve cells in an insect brain. *J. Exp. Biol.*, **49,** 171–183.

Saleh, B. E. A., Teich, M. C. (1982). Multiplied-Poisson noise in pulse, particle, and photon detection. *Proc. of the IEEE*, **70,** 229–245.

Saleh, B. E. A., Teich, M. C. (1985). Multiplication and refractoriness in the cat's retinal-ganglion-cell discharge at low light levels. *Biol. Cybern.*, **52,** 101–107.

Simmons, P. J. (1981). Ocellar excitation of the DCMD—an identified locust interneurone. *J. Exper. Biol.*, **91,** 355–359.

Simmons, P. J., Rind, F. C. (1992). The orthopteran DCMD neuron: a re-evaluation of responses to moving objects. II. Critical cues for detecting approaching objects. *J. Neurophysiol.*, **68,** 1667–1682.

Teich, M. C., Khanna, S. M. (1985). Pulse-number distribution for the neural spike train in the cat's auditory nerve. *J. Acoust. Soc. Am.*, **77,** 1110–1128.

Teich, M. C., Lowen, S. B. (1994). Fractal patterns in auditory nerve-spike trains. *IEEE Eng. Med. Biol. Mag.*, **13,** 197–202.

Teich, M. C., Turcott, R. G. (1988). Multinomial pulse-number distributions for neural spikes in primary auditory fibers: theory. *Biol. Cybern.*, **59,** 91–102.

Teich, M. C. (1989). Fractal character of the auditory neural spike train. *IEEE Trans. Biomed. Eng.*, **36,** 150–160.

Teich, M. C., Johnson, D. H., Kumar, A. R., and Turcott, R. G. (1990a). Rate fluctuations and fractional power-law noise recorded from cells in the lower auditory pathway of the cat. *Hearing Res.*, **46,** 41–52.

Teich, M. C., Turcott, R. G., and Lowen, S. B. (1990b). The fractal doubly stochastic Poisson point process as a model for the cochlear neural spike train. In: Dallos, P., Geisler, C. D., Matthews, J. W., Ruggero, M. A., and Steele, C. R. (eds). The mechanics and biophysics of hearing. Springer, New York, pp. 354–361.

Teich, M. C. (1992). Fractal neuronal firing patterns. In: McKenna, T., Davis, J., and Zornetzer, S. (eds). Single neuron computation. Academic, Boston, pp. 589–625.

Turcott, R. G., Lowen, S. B., Li, E., Johnson, D., Tsuchitani, C., and Teich, M. C. (1994). A nonstationary Poisson point process describes the sequence of action potentials over long time scales in lateral-superior-olive auditory neurons. *Biol. Cybern.*, **70,** 209–217.